Volume 1 | Number 1 | Jan 2013 | Pages 1–100

Journal of
Materials Chemistry C

Materials for optical and electronic devices
www.rsc.org/materialsC

ROYAL SOCIETY
OF CHEMISTRY

Journal of Materials Chemistry C

ARTICLE

Luminescence switch of Mn-Doped $ZnAl_2O_4$ powder with temperature

L. Cornu[a,b], M. Duttine[a,b,c,d], M. Gaudon*[a,b] and V. Jubera*[a,b]

Manganese-doped $ZnAl_2O_4$ phosphors were prepared by the Pechini synthesis route and treated at various temperatures (from 600 °C up to 1350 °C). The samples were characterized by TEM-EDX, XRD, EPR, and their diffuse reflectance and luminescence properties were investigated. The structural analysis shown the high solubility limit of manganese in this spinel matrix and allowed the determination of the global inversion rate which characterizes the cation distribution in both, A and B sites of the spinel structure. As the annealing temperature increases, this factor decreases leading to a more direct matrix. EPR analyzes evidenced that, besides Mn^{3+} to Mn^{2+} reduction, the local environment of Mn^{2+} cations change with the annealing temperature, what is also reflected in the evolution of the optical properties. As the annealing temperature increases, the red luminescence related to the presence of divalent manganese in octahedral sites fades away to be replaced by a new green emission due to Mn(II) ions located in tetrahedral sites within the spinel structure. For 0.5% Mn-doped $ZnAl_2O_4$, this red to green luminescence switch occurred for samples treated between 1200 °C and 1350 °C. Moreover, the study of Al-overstoichiometric samples $Mn:ZnAl_{2.2}O_{4+\delta}$ shows that it is possible to modify the temperature range and the kinetic of this variation of emission wavelength. Such tuneable properties lead to consider these Mn-doped spinels as potential candidates for developing stable and highly sensitive thermal sensors.

1. Introduction

Over the past decades, many applications of $ZnAl_2O_4$ spinel compounds have been reported for catalysis of hydrocarbon reaction,[1,2] sintering process of alumina ceramics,[3] or improving ceramic dielectric properties.[4,5] With an energy gap of 3.8 eV, this material is also a ultraviolet absorbent and is already used in optoelectronic devices.[6] Doped with transition metal ions such as cobalt,[7-9] manganese[10-12] or rare earth elements, *e.g.* europium[13] or terbium,[14] $ZnAl_2O_4$ spinel can be used, for example, as luminescent material in flat panel display[15] or as pigments in glazes or stoneware.[16] Indeed, its structure offers many possibilities of luminescence coloration (wavelength range of emission bands) by modulating the doping level and the location of the doping agent into the structure. Spinel compounds of general formula AB_2O_4 crystallize in the cubic system with space group Fd-3m. The unit cell contains 32 oxygen ions which form 64 tetrahedral sites and 32 octahedral sites. Each unit cell is composed of eight AB_2O_4 patterns. In the direct spinel structure, only 8 of the tetrahedral sites: wyckoff positions 8*a* (1/8, 1/8, 1/8) and 16 of the octahedral sites: wyckoff positions 16*d* (1/2, 1/2, 1/2), are

respectively occupied by the A and B cations and the oxygen anions fully occupy the 32*e* positions.[11] In $ZnAl_2O_4$, also called gahnite, a non-negligible quantity of Zn^{2+} cations is located in the 16*d* sites and as a consequence, Al^{3+} cations may partially occupy the 8*a* sites. The proportion of Zn^{2+} cations in octahedral site is called inversion rate (δ) and can take any value between 0 and 1. The general formula of such spinel phase can be written $(Zn_{1-\delta}Al_\delta)[Al_{2-\delta}Zn_\delta]O_4$ in which parentheses symbolize the tetrahedral sites and brackets the octahedral ones. In literature an inversion rate varying between $0 < \delta < 0.05$[17-19] is reported for the $ZnAl_2O_4$ matrix. Indeed, the value of δ was clearly shown to be dependent on the chosen synthesis route: solid-state reaction,[20-22] tartaric complex formation as the oxide precursor,[23] microwave-assisted hydrothermal process,[24] autocombustion using glycine/urea fuels,[14,25] sol-gel,[11] or Pechini route.[8,26] A special care must be taken with the nature of synthesis precursors and the accessible crystallite sizes as they both could impact the inversion rate of the as-prepared samples. We have recently demonstrated its evolution through Pechini and co-precipitation synthetic routes.[27] Controlling the inversion factor of doped $ZnAl_2O_4$

materials may be of great interest especially when the doping cation has luminescent properties which are sensitive to the crystal field strength and the coordination polyhedron, such as Mn^{2+}. Mn-doped materials have been intensively studied since the beginning of the twenty's century mainly because this transition metal ion presents an emission in the visible region and can be excited in many different ways. Luminescent emission consists of a broad band which illustrates the radiative de-excitation from the $^4T_1$ excited level to the $^6A_1$ ground state energy level. Mn^{2+} location in tetrahedral environment leads to a green centered emission whereas the luminescence is red-shifted for a location in an octahedron. A long decay time of the luminescence is expected because of the change in the spin multiplicity (from 100 µs to 1 ms).

In this work, Mn-doped $ZnAl_2O_4$ phases were prepared by a soft chemistry route (Pechini process) and treated at various temperatures in order to correlate cationic distributions and crystallite sizes. On one hand, Rietveld refinements performed on the samples XRD-patterns after various thermal treatments allow obtaining the global divalent cation inversion rate ($\delta_{Zn}+\delta'_{Mn}$, δ_{Zn} and δ'_{Mn} being the inversion rate of zinc and manganese cations respectively). On the other hand, to detect any changes in the specific Mn(II) environment, Electron Paramagnetic Resonance (EPR) analyses were performed. The combination of all these structural investigations and their correlation with luminescence properties leads to an accurate understanding of the influence of thermal treatment on the cationic distribution in Mn-doped $ZnAl_2O_4$ samples.

2. Materials and methods

2.1. Preparation of compounds. The $Zn_{(1-x)}Mn_xAl_2O_4$ samples were synthetized by the Pechini route. Stoichiometric amounts of zinc nitrate hexahydrate (Alfa-Aesar, Puratronic 99,998% (metal basis)), aluminum nitrate nonahydrate (Alfa-Aesar, low mercury, Puratronic 99,999% (metal basis)) and manganese nitrate hydrate (Alfa Aesar, Puratronic 99.999% (metal basis)) were dissolved in mineral water. Zinc concentration of the as-prepared solution is equal to 0.8 mol.L^{-1}. Then, citric acid (CA) and ethylene glycol (EG), used as polyesterification precursors, were added to the solution (salt:CA:EG molar ratios 1:4:4) and water is slowly evaporated by heating on a hot plate. The highly viscous mixture formed after polyesterification was annealed at 400 °C for 5 hours under air; a dark brown powder is thus obtained. Thereafter, various thermal treatments were performed between 500 °C and 1350 °C under air atmosphere during 10 hours. After this first thermal under air, the samples presented a light-yellow color. This coloration may reflect inter-valence absorption due to the presence of manganese in oxidation states higher than (II). An additional reductive thermal treatment under under argon/dihydrogen: 90 %mol–10 %mol atmosphere was then performed to reduce residual Mn(III) and Mn(IV) cations. The annealing temperature does not exceed 500 °C in order to avoid the occurrence of black spots on the powder surface and even inside the grains. This

localized dark coloring is probably due to the reduction of zinc or to the formation of colored centers associated to oxygen vacancies. Moreover, from a structural point of view, the highest concentration of manganese that can substitute zinc in the matrix was investigated.

2.2. X-ray Diffraction. Powder X-ray diffraction patterns have been collected on a Philips X'Pert MPD X-ray diffractometer with a Bragg-Brentano geometry and using Cu $K\alpha_{1,2}$ radiation ($10 < 2\theta < 130°$, step: 0.02° and counting time: 30 s). The diffractograms were analyzed with the Fullprof program package and structural model refinements were performed using the Rietvelt method with the conventional reliability factors. Unit cell parameters, atomic positions, occupancies and Debye-Waller factors have been refined on the basis of the *Fd-3m* space group corresponding to the spinel structure and considering the various composition models referred in the text. Furthermore, as the Fullprof peak profile function N°7 was used here, the crystallite size is directly obtained.

2.3. Transmission Electron Microscopy (TEM) and Energy-dispersive X-ray (EDX). Transmission Electron Microscopy was performed on TECNAI F20 equipment with a field emissive gun, operating at 200 kV and with a point resolution of 0.24 nm. TEM samples were prepared by dissolving few milligrams of powder in ethanol. The solution was then dipped ten minutes into an ultrasonic bath in order to disagglomerate and disperse powder particles. One drop of the solution was finally deposited on a Formvar/Carbon copper grid. Chemical cartographies were obtained using an EDX detector.

2.4. Photoluminescence. The photoluminescent properties were analyzed using a spectrofluorimeter SPEX FL212 equipped with a 450 W Xenon lamp. The excitation spectra were corrected for the variation of the incident flux as well as emission spectra for the transmission of the monochromator and the response of the photomultiplier. This equipment was also used to record diffuse reflectance spectra. In this case, the emission and the excitation monochromator are set in a synchronous mode, in order to collect all the diffuse reflection of the xenon lamp without catching any fluorescence photon. A black reference (*B*: blacktoner) and a white reference (*W*: Magnesia MgO) were scanned in the same condition and the measurement from the sample (*S*) was corrected to obtain the desired data (*D*) following the relation: $D = (S-B) / (W-B)$.

2.5. Electron Paramagnetic Resonance. EPR spectra were recorded at room temperature with a Bruker EMX spectrometer operating at X-band frequency (9.45 GHz). For the presented spectra, the main spectroscopic parameters are: microwave power 10 mW, magnetic field modulation frequency 100 kHz and amplitude 0.1 mT and spectral resolution 0.06 mT/pt. WINEPR and SIMFONIA softwares were used to simulate EPR spectra and estimate g values and hyperfine interaction parameters. DPPH was used as external reference to calibrate the spectrometer and $CuSO_4·5H_2O$ (Sigma Aldrich, 99.999% (metal basis)) as standard sample to estimate the number of spins participating in the observed resonances.

3. Results and discussion

3.1. Mn-solubility limit in $Zn_{1-x}Mn_xAl_2O_4$ phases. The XRD patterns of the two highly doped samples (x=0.15, x=0.30) show the characteristic diffraction peaks of the spinel structure (n°00-005-0669) (Fig. 1a and 1b). In addition, a secondary phase attributed to the α-Al_2O_3 phase (n°00-046-1212) was detected for the sample with the highest doping rate.
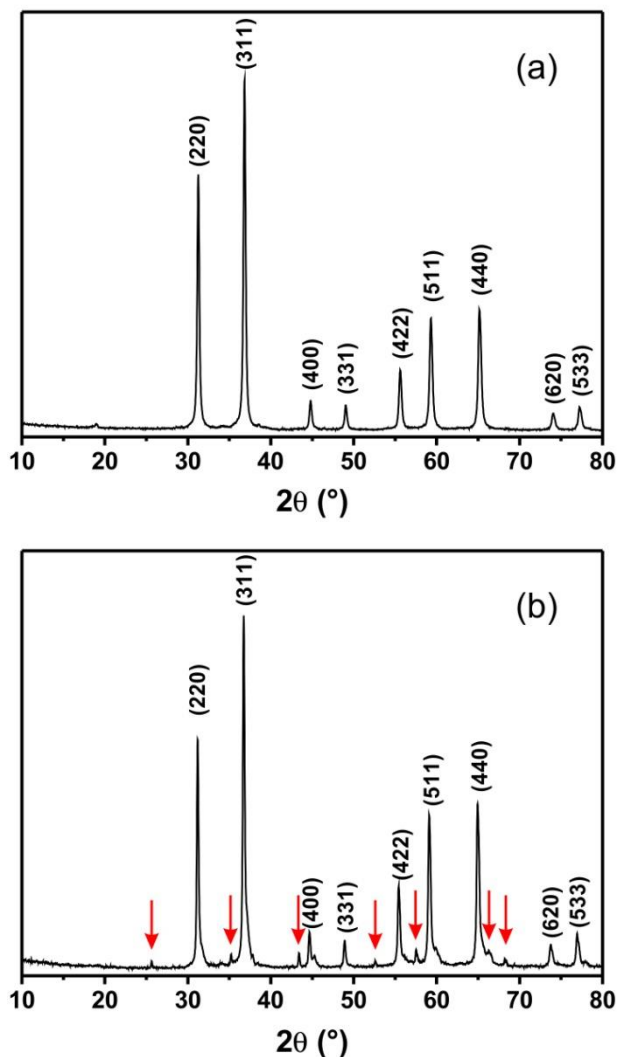
Fig. 1 X-ray Diffraction patterns of the 1000 °C treated samples with a) $Zn_{0.85}Mn_{0.15}Al_2O_4$ and b) $Zn_{0.7}Mn_{0.3}Al_2O_4$ composition. Red arrows show the secondary phase, α-Al2O3 corundum.

TEM-EDX analyses were performed on the two samples. For the 30% Mn-doped sample (Fig. 2a and 2b), the experimental atomic percentages vary significantly with the analyzed area. For instance, the analyzed area A (Fig. 2a) is more Zn^{2+}-rich than expected and the zinc/aluminum ratio is inverted compared to area B (Fig. 2b). Although the global composition of the whole polycrystalline aggregates are very close to the theoretical composition $(Zn_{0.7}Mn_{0.3}Al_2O_4)$, the intra-agglomerates inhomogeneity show the lack of miscibility of manganese and zinc in this region of the $ZnAl_2O_4$-$MnAl_2O_4$

binary phase diagram through the Pechini process here used. Moreover, at this Mn doping rate the limit of manganese and zinc miscibility is reached resulting in a compositional heterogeneity and in the formation of a secondary crystalline phase which is not a manganese oxide as expected, but an α-Al_2O_3 aluminate. Hence, the lack of miscibility for high manganese doping rate seems to be a consequence of a competition between the substitution of Mn^{2+} for Zn^{2+} and the substitution of Mn^{3+} for Al^{3+} (the $ZnMn_2O_4$ compound is also isotropic with the $ZnAl_2O_4$ one).

However, TEM-EDX analyses of the 15% Mn-doped sample (Fig. 2c) show that all the analyzed areas exhibit experimental Zn:Mn:Al ratios close to the theoretical ones, in good agreement with the XRD results revealing the crystallization of a single spinel phase. The manganese substitution of zinc in the $ZnAl_2O_4$ is thus limited to a value between 15% and 30%.

Atomic %	Zn	Mn	Al
zone A	56	14	30
zone B	34	14	52
zone C	30	5	65
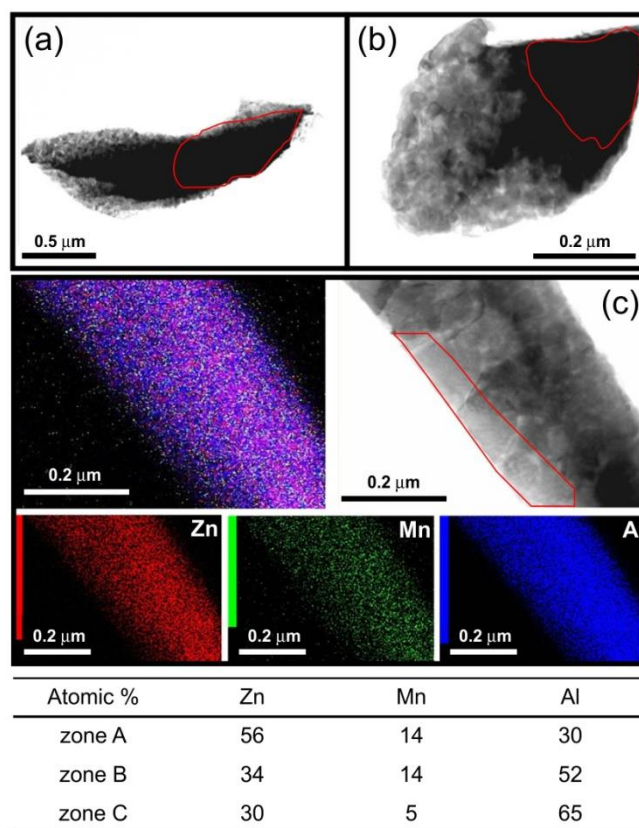
Fig. 2 a) and b) TEM images on aggregates of the 1000 °C treated samples with $Zn_{0.7}Mn_{0.3}Al_2O_4$ global composition, c) TEM images and EDX-cartographies of the 1000 °C treated sample with $Zn_{0.85}Mn_{0.15}Al_2O_4$ composition. Zn, Al and Mn molar percentages calculated from EDX data of A, B and C areas are given in the bottom table.

This first study has shown that occurrence of manganese III besides manganese II must be considered in our samples, with as consequences, a limit of manganese solubility about 15%.

Considering the optical behavior of Mn^{2+} and the low threshold of concentration quenching in this matrix, we have explored the luminescent properties of a 0.5% doped compound i.e. a value

This journal is © The Royal Society of Chemistry 2012

J. Mat. Chem. C, 2015, **00**, 1-3 | **3**

largely under the manganese solubility limit. All the discussed properties should then be attributed only to the spinel phase.

3.2. Global divalent cation inversion rate ($\delta_{Zn} + \delta'_{Mn}$) from XRD pattern refinements.

Rietveld refinements were performed on 0.5%Mn-doped $ZnAl_2O_4$ samples obtained after thermal treatments at temperature ranging from 500 °C to 1350 °C. Experimental and calculated spectra of the samples annealed at 600 °C and 1200 °C are presented by the Figure 3, for illustration.

Fig. 3 Refined X-ray diffractograms (experimental, calculated and difference) for
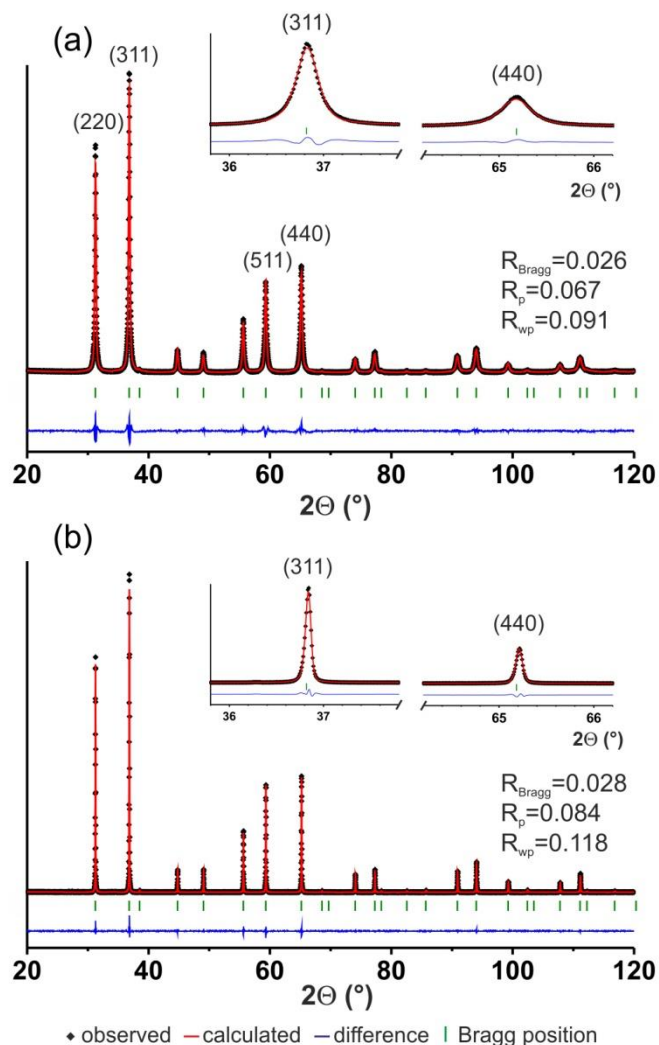
0.5%Mn-doped $ZnAl_2O_4$ samples obtained after thermal treatments respectively at a) 600 °C and b) 1200 °C.

As shown by the X-ray spectra of the Figure 3, a pure spinel form is obtained whatever the synthesis temperature. Considering the composition formulae: $(Zn_{0.995-\delta}Mn_{0.005-\delta'}Al_{\delta+\delta'})[Zn_\delta Mn_{\delta'}Al_{2-\delta-\delta'}]O_4$, only the global inversion rate $(\delta+\delta')$ of A^{2+} divalent cations can be determined from X-ray refinements. Indeed, the low doping level in Mn^{2+} ions and moreover, the proximity of the atomic number of Mn and Zn don't allow to accurately estimate the manganese occupancies.

Structural refinements were thus performed considering the following chemical formula: $(Zn_{1-\delta-\delta'}Al_{\delta+\delta'})[Zn_{\delta+\delta}Al_{2-\delta-\delta}]O_4$. Evolution of cell parameter, crystallite size and inversion rate with annealing temperature are presented in Table 1 and Fig. 4. The annealing temperature has a notable effect on the crystallite size and also, on the global inversion rate whereas no significant variation of cell parameter was observed. As the temperature increases, the sintering effect induces the crystallites growth from about 20 nm (at 500 °C) up to 120 nm (at 1350 °C) and the global inversion rate decreases gradually from 16% to 2.6% (Fig. 4). The impact of crystallite size on the cationic distribution seems secondary: the crystallite size almost doubles between 1000 °C and 1200 °C whereas the inversion rate remains stable. *A contrario*, annealing temperature appears to play a key role in the cationic distribution within the spinel structure and as a consequence, may influence the optical properties of the treated samples.

Table 1. Structural parameters of the 0.5% Mn-doped $ZnAl_2O_4$ samples obtained after various thermal treatments.

Synthesis T°	Crystallite size (nm)	Cell parameter (Å)	Inversion rate* (%)	Reliability factors**		
				Rp	χ^2	R-Bragg
500 °C	22.9	8.09(5)	15.9	0.051	4.0	0.042
600 °C	32.4	8.08(9)	8.7	0.067	5.0	0.026
800 °C	41.5	8.09(5)	5.9	0.058	4.0	0.028
1000 °C	54.9	8.084(5)	4.8	0.061	3.8	0.023
1200 °C	115.6	8.089(4)	4.7	0.084	2.5	0.028
1350 °C	119.3	8.087(4)	2.6	0.121	2.2	0.039

*global inversion rate $(\delta + \delta')$, **with all-non excluded model and not corrected for background.
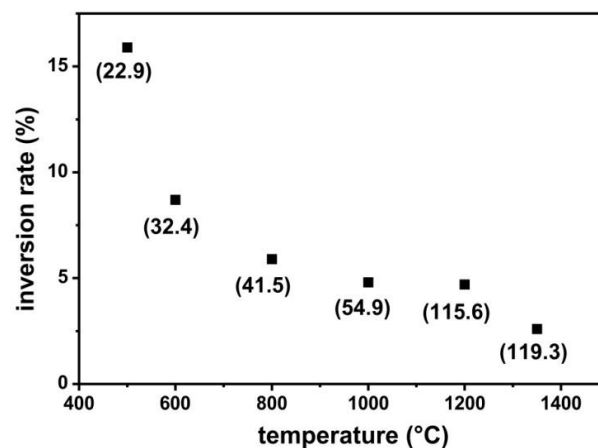
Fig. 4 Global A^{2+} divalent cations inversion rate versus the temperature of the post-thermal treatment for the 0.5% Mn-doped $ZnAl_2O_4$ sample. The 0.5% Mn-doped $ZnAl_2O_4$ crystallite sizes (in nm) are reported between parentheses.

3.3. Optical properties.

The optical properties of Mn-doped $ZnAl_2O_4$ depend on the location of Mn^{2+} ions within the spinel network. This phosphor ion substituted for Zn^{2+} may occupy octahedral and/or tetrahedral sites depending on synthesis parameters, especially the annealing temperature (as evidenced above). In a previous work[27], we underlined the influence of

4 | *J. Mat. Chem. C*, 2015, **00**, 1-3

This journal is © The Royal Society of Chemistry 2012

annealing temperature on the optical properties of non-doped $ZnAl_2O_4$ synthesized using the Pechini route. A drastic change in the diffuse reflectance spectra was observed as temperature increases from 1200 °C to 1350 °C. This last thermal treatment led to the total migration of zinc cations into the tetrahedral coordination polyhedra, a blue shift of the front absorption from 400 nm to 300 nm was then observed. Figure 5 shows diffuse reflectance spectra of manganese doped $ZnAl_2O_4$ as a function of the doping level for samples annealed at 1200 °C and 1350 °C.
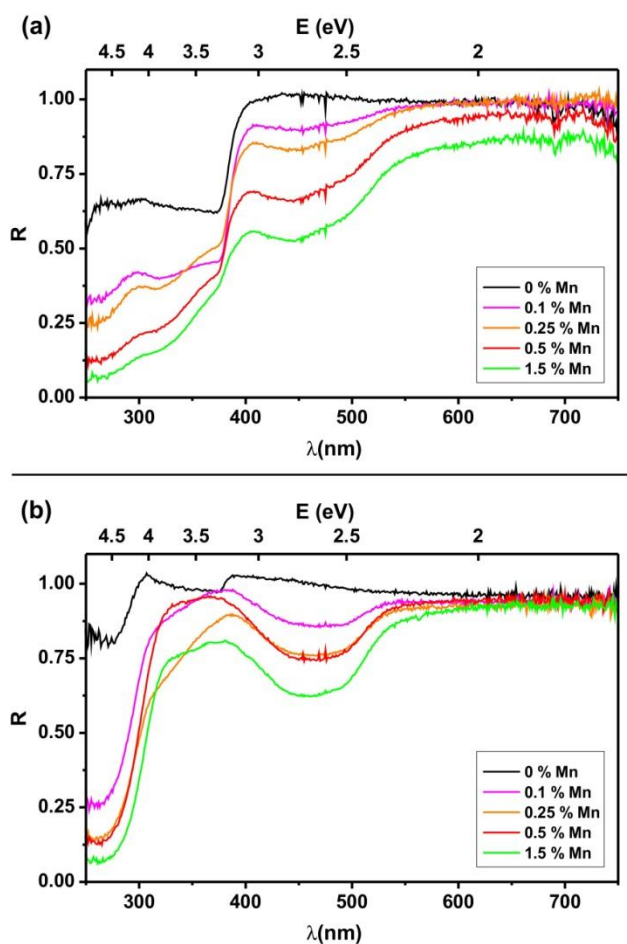
Fig. 5 Diffuse reflectance spectra of various Mn-doped $ZnAl_2O_4$ samples for different Mn^{2+} concentration obtained after thermal treatment at 1200 °C (a) and at 1350 °C (b).

As observed for the non-doped matrix, the contribution of Zn-O charge transfer band for the six fold-coordinated zinc ions located at 400 nm disappears after the 1350 °C heat-treatment. The Zn-O charge transfer that occurs in the tetrahedral zinc environment is then visible at 300 nm. Larger the amount of manganese, larger the absorption centered at 460 nm. Considering the low probability of the 3d-3d forbidden transition for divalent manganese, this band is probably due to inter-valence absorption or to manganese ions at a higher oxidation state. The depletion of aluminum from the spinel phase discussed earlier could be responsible for the occurrence of trivalent or tetravalent Mn^{n+}, ($R_{Mn3+} = 0.66$ Å;

$R_{Mn4+} = 0.54$ Å) may easily replace Al^{3+} ($R_{Al3+} = 0.53$ Å) in an octahedral environment.
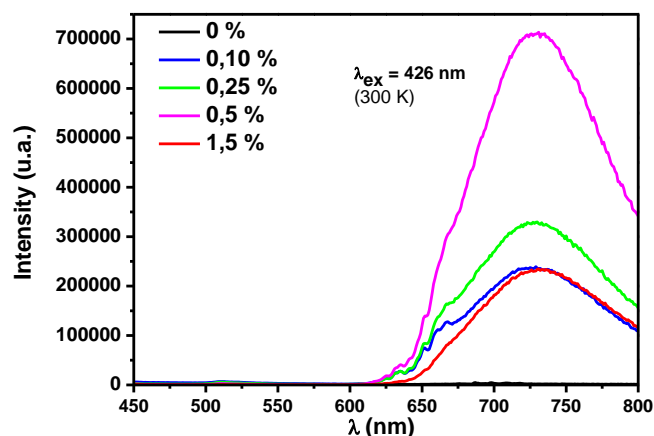
Fig. 6 Luminescence spectra of various Mn-doped $ZnAl_2O_4$ heat treated at 800°C under air and annealed under argon – hydrogen at 500°C.

The luminescence spectra of various Mn-doped compositions recorded at 300 K for the optimal excitation wavelength at 426 nm, are joined in the Figure 6. Despite the occurrence of defects in the spinel compounds obtained at this thermal treatment temperature, with a non-negligible associated photoluminescence (PL) phenomenon as shown into our previous work,[27] in direct comparison with Mn-doped compounds, the $ZnAl_2O_4$ matrix appears as non-luminescent for an excitation at 426 nm. It can be clearly seen that all the compositions roughly exhibit the same spectral distribution (same Gaussian shape centered on the same wavelength) with only the intensities diverging. The 0.5 mol.% Mn-doped compound gets the higher photoluminescence response. The dependency of the PL intensity versus the doping element concentration is usually described for luminescent materials: it shows a concentration quenching threshold at about 0,5% of molar substitution. Thus, it was decided to concentrate the characterization studies on the optimal compound for accurate description.

The next part of the study will be focused on the 0.5% doped material. Evolution of the absorption with the annealing temperature is presented by Figure 7. A drastic change in the diffuse reflectance spectra being observed for T > 1200 °C, only the 1200 °C and 1350 °C heat-treatments will be discussed thereafter. Figure 8 shows the excitation and emission spectra recorded for the samples obtained after annealing at these two temperatures.

At 1350 °C, the total direct Mn-doped spinel present the expected green luminescence (see Fig. 8c) reported in many papers for a tetrahedral environment of divalent manganese.[28-31] Considering the "site preference energies" of Mn^{2+} and Al^{3+} (-14.7 kcal/m and -2.5 kcal/m respectively), divalent manganese ions may preferentially occupy a tetrahedral coordination.[32] The main $^4T_1 \rightarrow ^6A_1$ transition peaks at 508 nm and sidebands vibronic vibrations are detected at lower energy.

This journal is © The Royal Society of Chemistry 2012

J. Mat. Chem. C, 2015, **00**, 1-3 | **5**

They peak at 514 nm, 520 nm and 529 nm respectively. Table 2 lists the splitting of the different energy level observed at 10 K (Fig. 8c). The $^6A_1 \rightarrow {}^4T_1({}^4G)$ absorption component is not observed because the Stokes shift is too small and the experimental acquisition conditions not appropriate. The $^6A_1 \rightarrow {}^4T_{2g}({}^4G)$ triplet absorption line is well resolved whereas a unique line is detected for the $^6A_1 \rightarrow {}^4E_g/{}^4A_{1g}$ $({}^4G)$ transitions. Finally two doublet can be attributed to the $^6A_1 \rightarrow {}^4T_{2g}({}^4D)$ and $^6A_1 \rightarrow {}^4E_g({}^4D)$ transitions. The decay time value of this green emission is equal to 4.8 ms (measurement performed for an excitation at 426 nm and an emission at 510 nm), which is close to the values reported in literature.[33] Value was calculated using a bi-exponential fitting model. A secondary faster component (0.3 ms) is also observed indicating a competitive de-excitation phenomenon that might be due to matrix defect.
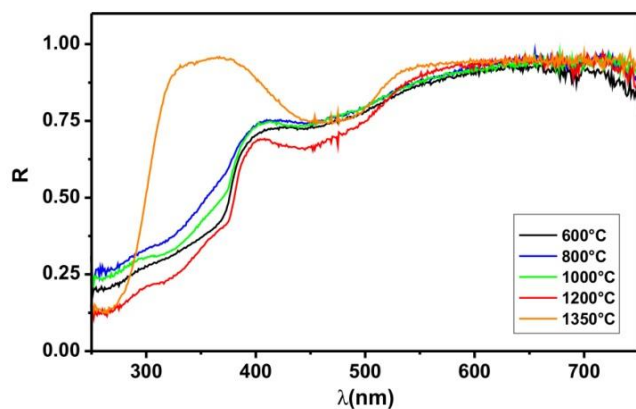
Fig. 7 Diffuse reflectance spectra of 0.5% Mn-doped ZnAl$_2$O$_4$ samples obtained after various thermal treatments.

For an excitation at 426 nm, red emission lines were also detected between 640 nm and 730 nm. Considering the diffuse reflectance spectra of doped (Fig. 7) and non-doped ZnAl$_2$O$_4$ matrix,[27] these emission lines are due to trace of Cr^{3+} luminescence, as observed in the non-doped materials. Isoelectronic Mn^{4+} could also contribute to this emission.. Presence of Mn^{4+} will be discussed latter. However, due to the high similarity of the two spectral distributions, their respective contribution to the whole spectrum cannot be separated, at least with these experimental conditions.

The luminescence properties of the sample annealed at 1200 °C revealed that a significant amount of manganese ions are not four-fold coordinated (Fig. 8a). The emission spectrum obtained under a 426 nm excitation clearly show a large band centered at 738 nm. Emission spectrum of the non-doped matrix confirms the fact that this red luminescence is related to the introduction of manganese within the partially indirect spinel network. As demonstrated in previous investigation,[27] the optical properties of the 1200 °C heat treated spinel are directly linked to the occurrence of punctual defects. A red luminescence obtained for an excitation at 370 nm has been related to the presence of oxygen vacancies in the vicinity of Zn$_{Al}$ antisite. This emission isn't observed with an excitation at 426 nm. Then a part of manganese ions with valence higher than two could be localized either in these distorted five-fold coordinated polyhedra or in regular AlO$_6$ octahedra, substituting for Al^{3+}. Mn^{4+} luminescence have already been mentioned in the previous paragraph. Moreover, no additional spectral distribution due to Mn^{3+} was observed. Nevertheless, even if Mn^{3+} was stabilized in this matrix, the associated luminescence could not be observed because of a strong Jahn-Teller effect.[29] From the above statements, we assume that the reducing heat-treatment applied during the chosen synthetic route has successfully stabilized divalent manganese ions in anti-site (divalent cation in the Al^{3+} site) with coordination number higher than 4, leading to the red emission observed for the Mn-doped ZnAl$_2$O$_4$ spinels. Moreover, the shape of the excitation spectrum (large component) indicates that the crystallographic environment of the doping ions is not well-defined and regular. Decay time measurements were performed for excitation and emission wavelengths equal to 426 nm and 735 nm respectively. The experimental decay curve was decomposed into two equally weighted components with different decay time values, 50 µs and 250 µs, close to those already reported for red emission of Mn^{2+}.[34]

The modification of the optical transition rules when changing the symmetry around the element (more strictly parity forbidden). This observation doesn't exclude the fact that part of the divalent manganese should be localized in the tetrahedra. A zoom in the 450-650 nm range (Fig. 8b) show clearly a weak green emission but regarding the spectral distribution of the excitation spectrum of the red luminescence, we can conclude that if existing, this green emission is mainly reabsorb

Table 2. Splitting of Mn^{2+} energy levels in ZnAl$_2$O$_4$.

Energy level of free Mn^{2+} ion (3d^5)	Energy level in T$_d$ or O$_h$ sites	Observed transitions / excitation in nm (cm^{-1})	
		1350 °C-annealed compound (4-fold coordinated Mn^{2+})	1200 °C-annealed compound (5/6-fold coordinated Mn^{2+})
^4G	$^4T_{1g}$	Not observed	Not observed
	$^4T_{2g}$	434 (23041)<λ_{ex}<475 (21052)	462 (21645)<λ_{ex}<559 (17889)
	$^4E_g/{}^4A_{1g}$	428 (23364)	434 (23041)
^4D	$^4T_{2g}$	388 (25773)	369 (27100)
	^4E_g	363 (27548)	352 (28409)

6 | *J. Mat. Chem. C*, 2015, **00**, 1-3

This journal is © The Royal Society of Chemistry 2012
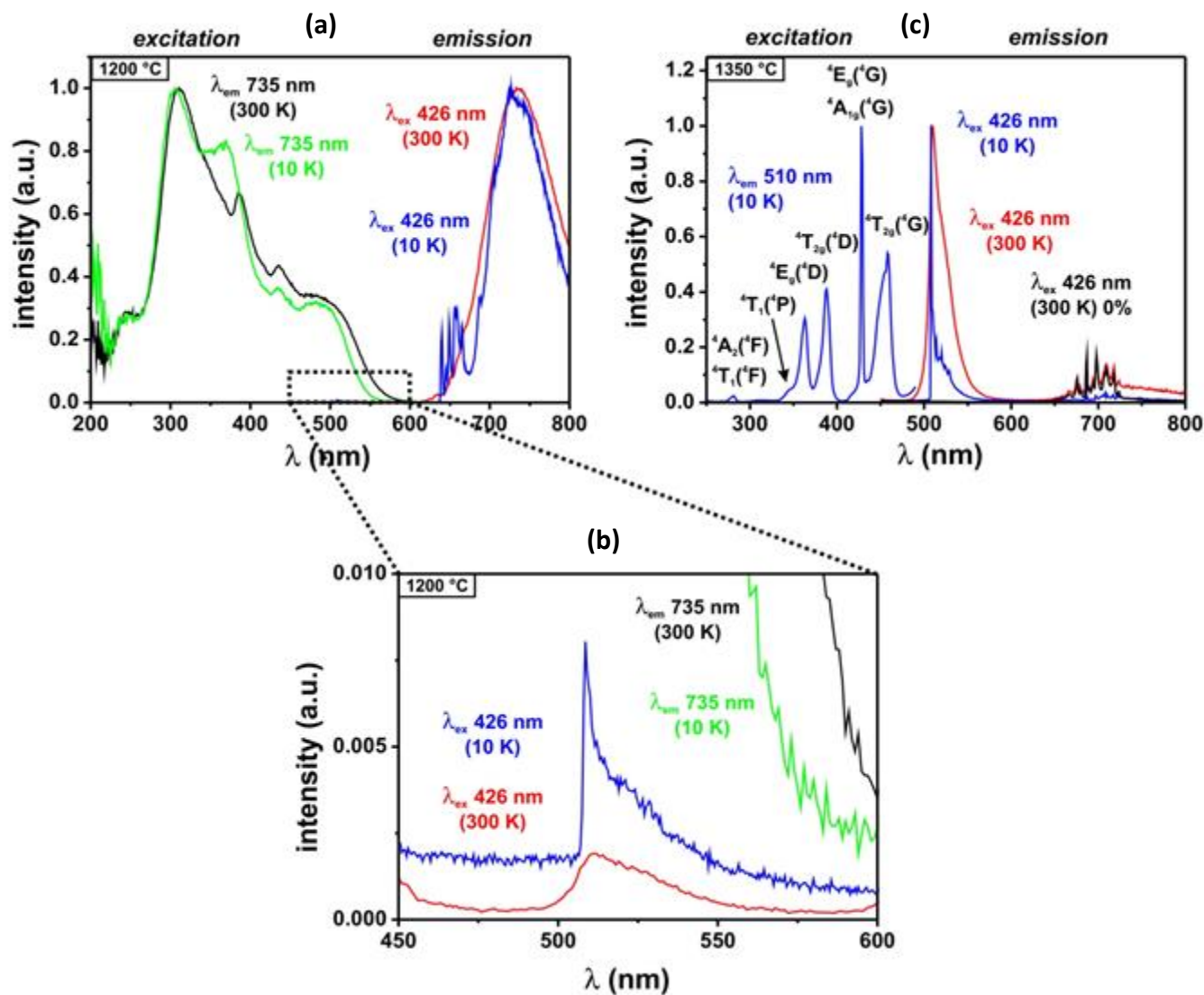
Fig. 8 Luminescence spectra of the 0.5% Mn-doped $ZnAl_2O_4$ sample after thermal treatment at 1200°C (a) and (b) (zoom on the 450-600 nm range) and 1350°C (c).

3.4. Al-overstoichiometric phases, $Zn_{0.995}Mn_{0.005}Al_{2.2}O_{4+\delta}$.

In order to better understand the coupling between octahedral occupancy of manganese and temperature, a compound presenting an excess of aluminum atoms was prepared. A 0.5% Mn-doped $ZnAl_{2.2}O_4$ sample was heat-treated at 800 °C, 1000 °C and 1200 °C. The over-stoichiometry of oxygen is obviously remained to simplify the description; the anionic sub-network into spinel forming a slightly distorted rocksalt-like anionic framework, supplementary anions could not be inserted within the structure. Actually, the compensation of Al-overstoichiometry is achieved from cationic vacancies in both tetrahedral and octahedral sites. The crystallite sizes calculated by Rietveld refinement are equal to 27 nm, 40 nm and 58 nm from the lowest to the higher thermal treatment, respectively. The corresponding inversion rates are weaker than those calculated for the stoichiometric sample. 2.92%, 1.20% and 0% were determined, the lowest inversion rate being associated to the highest temperature, which indicates that to introduce a divalent cation in the octahedral position is more difficult.

This journal is © The Royal Society of Chemistry 2012

J. Mat. Chem. C, 2015, 00, 1-3 | 7
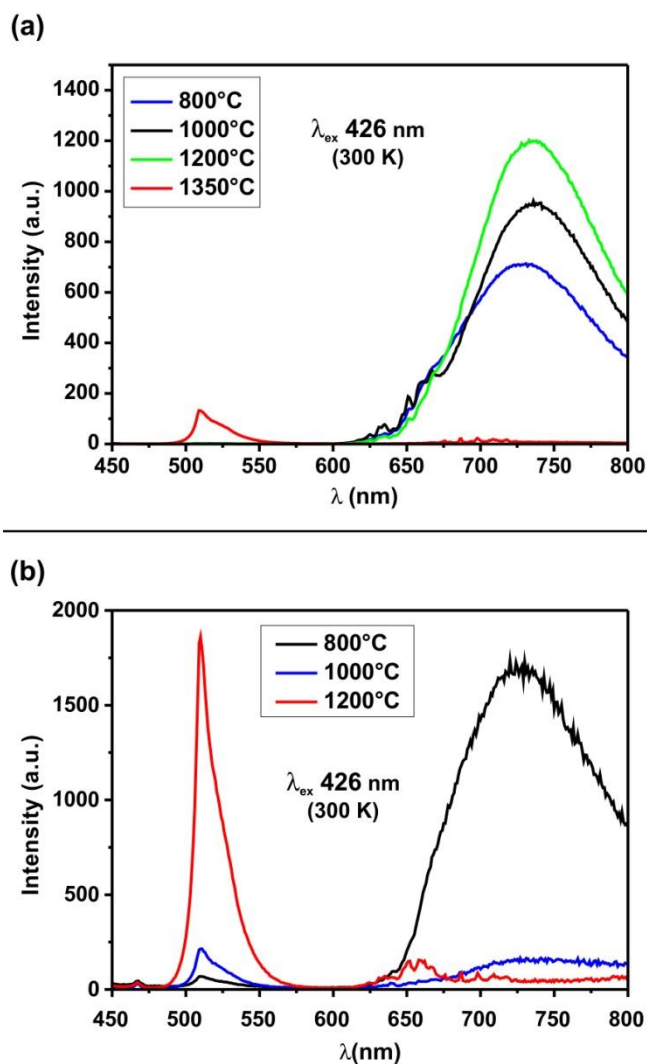
Fig. 9 Luminescence spectra of 0.5% Mn-doped (a) $ZnAl_2O_4$ and (b) $ZnAl_{2.2}O_{4+\delta}$ samples annealed at various temperatures.

temperature opening a wide panel of applications for these material series as thermal sensors.

3.5. Electron Paramagnetic Resonance study. Polycrystalline samples of 0.5 %mol. Mn-doped $ZnAl_2O_4$ and $ZnAl_{2.2}O_{4+\delta}$ annealed at temperatures ranging from 800 °C to 1350 °C were analyzed by EPR spectroscopy.
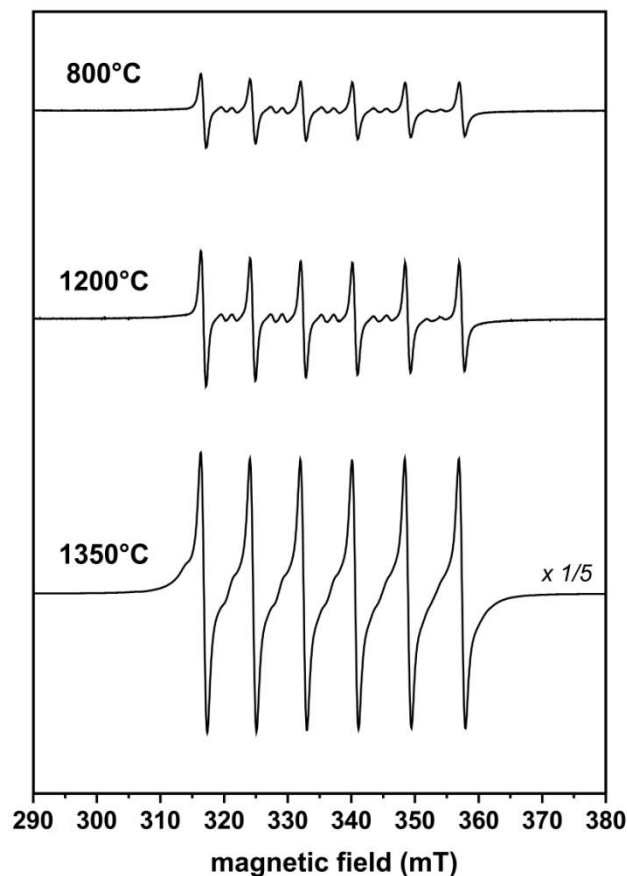
Fig. 10 Room temperature X-band EPR spectra of 0.5% Mn-doped ZnAl2O4 annealed at 800 °C, 1200 °C and 1350 °C.

Regarding the new luminescent properties (Fig. 9), divalent manganese cations migration from the octahedral to the tetrahedral location is detected from 800 °C and is complete at 1200 °C. The relative maximum intensity between the two luminescences varies from 0.042 (I_{max510}/I_{max733} 800 °C) , 1.41 (1000 °C) to 40.43 (1200 °C) for the Al^{3+}-overstoichiometric sample in comparison with a value equal to 0.006 for the 1200 °C-annealed stoichiometric sample (see Figure 9). For Mn-doped $ZnAl_{2.2}O_4$ materials, a larger temperature range is accessible to modulate the expected visible emission. The evolution of luminescence properties versus thermal treatment temperature is clearly directly correlated to the stabilization of the manganese cations into tetrahedral sites. Hence, from an adequate variation of the matrix chemical composition, knowing and "playing" with the preferential octahedral or tetrahedral site occupancy of the constituting cations, the red to green emission switch can be clearly tuned at lower

The spectra presented by Figures 10 and 11 are characteristic of Mn^{2+} ions ($3d^5$: ^6S ground state, S=5/2, I=5/2) and can be described by the spin Hamiltonian:

$$\mathcal{H} = g\beta H \cdot S + S \cdot D \cdot S + AS \cdot I \qquad (1)$$

The first term of Eq. (1) represents the Zeeman interaction where g is the g factor, β the Bohr magneton and H the applied magnetic field. The second term is the zero-field splitting term which can be written

$$D\left[S_z^2 - \frac{1}{3}S(S+1)\right] + E\left(S_x^2 - S_y^2\right) \qquad (2)$$

where D and E are the zero-field splitting parameters ($-1 \leq 3E/D \leq 0$ in the standard range). And, the third term arises from the hyperfine interaction with the Mn nuclear spin (I) where A is the hyperfine coupling constant whose value is directly linked to the ionicity of the metal − ligand bonds (at least when Mn^{2+} is in a cubic or nearly cubic crystal field).[35] In

8 | *J. Mat. Chem. C*, 2015, **00**, 1-3

This journal is © The Royal Society of Chemistry 2012

this work, the g factor and the hyperfine coupling constant can be reasonably considered isotropic and, according to previous studies[36] the cubic zero-field splitting term that could be added to the spin Hamiltonian (1) is neglected.
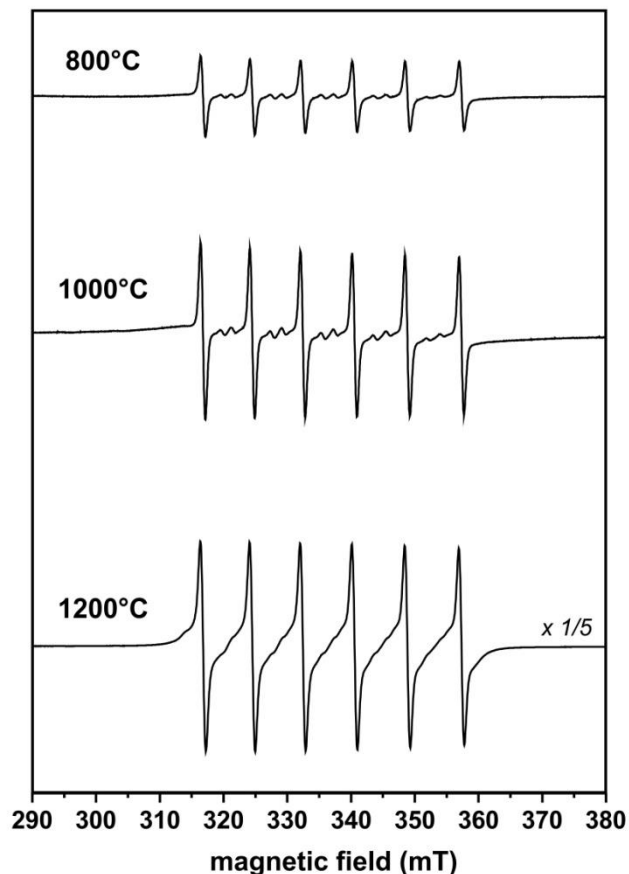
Fig. 11 Room temperature X-band EPR spectra of 0.5% Mn-doped $ZnAl_{2.2}O_{4+\delta}$ annealed at 800 °C, 1000 °C and 1200 °C.

The Mn^{2+} EPR signal consists of six (2I+1) main lines (Fig. 10 & 11) corresponding to the allowed transitions ($\Delta m=0$) between $|+1/2, m\rangle$ and $|-1/2, m\rangle$ levels where m is the nuclear spin magnetic quantum number, $-5/2 \leq m \leq +5/2$. The other four allowed transitions ($\Delta M=\pm 1$, $\Delta m=0$; M, electronic spin magnetic quantum number, $-5/2 < M \leq +5/2$) are strongly dependent of the zero-field splitting terms D and E in first order and are generally not resolved in powder spectra. In between each of the six allowed lines, the five doublets are associated to forbidden transitions ($\Delta m=\pm 1$) arising from the second order perturbation of the nuclear hyperfine levels by the zero-field splitting.[37] According to Shaffer et al.,[38] the ratio of the intensities of the forbidden lines I_f to the allowed ones I_A is given by Eq. (3), obtained by neglecting the E term of the spin Hamiltonian (Eq. (1)).

$$\frac{I_f}{I_A} = \frac{512}{15}\left(\frac{35}{4} - m^2 + m\right)\left(\frac{D^*}{g\beta H}\right)^2 \qquad (3)$$

This parameter can also be roughly estimated from polycrystalline EPR spectra by measuring the relative intensities of the allowed lines.[39,40] Nevertheless, an accurate evaluation of the D and E values generally requires EPR analysis of single crystals.

The $g = 2.0015 \pm 0.0002$ and $|A| = 76 \pm 1 \times 10^{-4}$ cm^{-1} values calculated for the observed signals (Table 3) are close to those already reported for Mn^{2+} ions in ZnO[41] in $MgAl_2O_4$[38,42] and $ZnAl_2O_4$[25,36] spinels where Mn^{2+} is assumed to be substituted for the divalent cation at tetrahedral A sites of the spinel structure. It is worth mentioning that the assignment to octahedral or tetrahedral site is quite difficult without complementary information (structural features or optical properties, for example).

However, none of the samples exhibits Mn^{4+} ($3d^3$: $^4A_2$ ground state, S=3/2, I=5/2) signal whose g-value (1.994 ± 0.001);[43,44] differs significantly from Mn^{2+} one (g > 2.000).[45] Then, the increase of EPR signal intensity with annealing temperature (Fig. 10) may be due to the reduction of Mn^{3+} ($3d^4$, EPR silent) to Mn^{2+}, what appears to be fully achieved after a thermal treatment at 1350 °C. As a matter of fact, the number of spins responsible for the EPR signal of the 1350 °C-annealed Mn:ZnAl$_2$O$_4$ sample corresponds to 0.49(8) molar percent of Mn^{2+} ions close to the initial Mn doping level (Table 3). Moreover, for the Mn-doped $ZnAl_{2.2}O_{4+\delta}$, only half of the manganese ions are at the +II oxidation state after a thermal treatment at 1200 °C (Table 3), revealing the influence of the annealing temperature on the Mn^{2+}/Mn^{3+} ratio within the spinel matrix. A similar evolution of Mn^{2+} EPR signal with temperature was reported by Su Kim et al.[46] for Mn-doped $ZnGa_2O_4$ phosphors annealed at temperatures ranging from 700 °C to 1100 °C.

From a crystallographic point of view, Mn^{3+} ions would preferentially occupy the octahedral B sites and Mn^{2+} the tetrahedral A sites, considering the oxidation states and the ionic radii of the doping ions (Mn^{2+}: 0.80 Å; Mn^{3+}: 0.66 Å) and

This journal is © The Royal Society of Chemistry 2012

J. Mat. Chem. C, 2015, **00**, 1-3 | **9**

substituted cations (Zn^{2+}: 0.74 Å; Al^{3+}: 0.53 Å). However, we previously showed that the cationic distribution within the $ZnAl_2O_4$ matrix and the occurrence of punctual defects (*e.g.* oxygen vacancies) are clearly influenced by the annealing temperature (Fig. 4). Thus, Mn-doped $ZnAl_2O_4$ samples annealed at $T \leq 1200\ °C$ may contain Mn^{2+} ions in anti-sites

(B sites) with a coordination number higher than 4. The resulting distortion of the manganese environment may then induce a significant change in the Mn^{2+} EPR signal, *i.e.* increase of the forbidden lines intensity and modification of the relative intensities of the allowed hyperfine lines.

Table 3. EPR parameters for Mn^{2+} signal in 0.5% Mn-doped $ZnAl_2O_4$ and 0.5% Mn-doped $ZnAl_{2.2}O_{4+\delta}$ obtained after various thermal treatments. g factor, hyperfine coupling constant $|A|$, "zero-field splitting parameter" D^*, peak-to-peak linewidth ΔH_{pp} and number of spins N (associated to the observed signal)

Synthesis T°	g factor	$\|A\|$ (x 10^{-4} cm^{-1})	D^* (x 10^{-4} cm^{-1})	ΔH_{pp} (mT)	N (x 10^{20})	[Mn^{2+}] (%*mol.*)
0.5% Mn-doped $ZnAl_2O_4$						
800 °C	2.0016(2)	76(1)	58(2)	0.6(1)	0.026(1)	0.016(1)
1200 °C	2.0015(2)	76(1)	49(2)	0.6(1)	0.048(2)	0.029(1)
1350 °C	2.0014(2)	76(1)	26(1)	1.0(1)	0.804(8)	0.490(8)
0.5% Mn-doped $ZnAl_{2.2}O_{4+\delta}$						
800 °C	2.0016(2)	76(1)	45(2)	0.7(1)	0.022(1)	0.013(1)
1000 °C	2.0015(2)	76(1)	34(1)	0.7(1)	0.038(1)	0.023(1)
1200 °C	2.0013(2)	76(1)	10(1)	0.8(1)	0.382(9)	0.235(8)

From the above statements, we assume that the EPR spectra presented on Figures 10 and 11 are the sum of two signals associated to 4-fold and 5/6-fold coordinated Mn^{2+} ions, respectively. As the annealing temperature increases, the global divalent cation inversion rate and the amount of defects (oxygen vacancies) decrease, thus, the relative proportion of these two EPR signals may change. Indeed, the signal of Mn^{2+} becomes more regular, as reflected by the decrease of D^* parameter (Table 3), revealing a less distorted environment for Mn^{2+} ions. Then, the EPR spectra of the samples annealed at high temperature (1350 °C for Al-stoichiometric samples and 1200 °C for Al-overstoichiometric samples) can be associated to Mn^{2+} ions in tetrahedral site (Zn^{2+} site) within a direct spinel structure. This is in good agreement with the optical properties showing a drastic increase of the T_d-Mn^{2+} emission for the Mn-doped $ZnAl_2O_4$ spinels annealed at 1350 °C and for the Mn-doped $ZnAl_{2.2}O_{4+\delta}$ phosphors synthesized at 1200 °C (see previous section).

4. Conclusions

This study shows that the thermal history of $ZnAl_2O_4$ spinels doped with manganese ions has a strong influence on their optical properties. The structural features of the as-prepared samples indicate that the solubility limit is reached for a high manganese concentration (between 15 and 30 mol%). Moreover, the cationic distribution for 0.5mol%-doped $ZnAl_2O_4$ samples obtained after various thermal treatments was monitored by XRD and EPR analyses. From XRD data, the structural refinements show that the global inversion rate (Zn+Mn) decreases with the annealing temperature. EPR investigations revealed a clear change of Mn^{2+} local environment within the spinel matrix and also, the increase of Mn^{2+} amount, due to the reduction of Mn^{3+} ions. The divalent manganese cations progressively and irreversibly migrate from

the octahedral sites to the tetrahedral ones. As shown here, the variations of luminescence properties are directly correlated to the inversion rate evolution. The samples treated at low temperatures exhibit a red luminescence characteristic of manganese in octahedral sites. As the annealing temperature increases, the inversion rate decreases and a green emission associated to divalent manganese ions in tetrahedral environment is observed. Furthermore, it has been pointed out that a low amount of manganese in octahedral sites is required to prevent any re-absorption phenomena that could reduce or quench the green luminescent emission. Finally, the temperature range and the kinetic of this luminescence switch can be modified by modulating the spinel matrix composition. The capability of this material to irreversibly change of luminescence properties according to its thermal history leads us to consider its use as a thermal sensor.

Notes and references

[a]CNRS, ICMCB, UPR 9048, F-33600 Pessac, France.
[b]Univ. Bordeaux, ICMCB, UPR 9048, F-33600 Pessac, France.
[c]Sorbonne Universités, UPMC Univ Paris 06, UMR 8234, PHENIX, F-75005, Paris, France.
[d]CNRS, UMR 8234, PHENIX, F-75005, Paris, France.
*Corresponding authors, email: gaudon@icmcb-bordeaux.cnrs.fr and jubera@icmcb-bordeaux.cnrs.fr

10 | *J. Mat. Chem. C*, 2015, **00**, 1-3

This journal is © The Royal Society of Chemistry 2012

1   J. Wrzyszcz, M. Zawadzki, J. Trawczynski, H. Grabowska and W. Mista, *Applied Catalysis A: General*, 2001, **210**(1-2), 263.

2   F. Le Peltier, P. Chaumette, J. Saussey, M.M. Bettahar and J.C. Lavalley, *Journal of Molecular Catalysis A: Chemical*, 1997, **122**(2-3), 131.

3   T.K. Parya, R.K. Bhattacharyya, S. Banerjee and U.B. Adhikari, *Ceramics International*, 2010, **36**(4), 1211.

4   C. Angeletti, F. Pepe and P. Porta, *Journal of the Chemical Society, Faraday Transactions 1,* 1977, **73**, 1972.

5   Jia-Min Lu, When-Zhong Lu, Wen Lei and Xiao-Chaun Wang, *Materials Research Bulletin*, 2011, **46** (9), 1485.

6   S.K. Sampath and J.F. Cordaro, *Journal of American Ceramic Society*, 1998, **81**(3), 649.

7   A. Fernandez-Osorio, E. Pineda-Villanueva and J. Chavez-Fernandez, *Materials Research Bulletin*, 2012, **47**(2), 445.

8   M. Gaudon, A. Apheceixborde, M. Menetrier, A. Le Nestour and A. Demourgues, *Inorganic Chemistry*, 2009, **48**(19), 9085.

9   A. Le Nestour, M. Gaudon, G. Villeneuve, M. Daturi, R. Andriessen and A. Demourgues, *Inorganic Chemistry*, 2007, **46**(10), 4067.

10 Mu-Tsun Tsai, Yu-Feng Lu and Yen-Kai Wang, *Journal of Alloys and Compounds*, 2010, **505**(2), 818.

11 J. Popovic, B. Grzeta, B. Rakvin, E. Tkalcec, M. Vrankic and S. Kurajica, *Journal of Alloys and Compounds*, 2011, **509**(34), 8487.

12 Mu-Tsun Tsai, Yee-Shin Chang, Ing-Bang Huang and Bo-Yu Pan, *Ceramics International*, 2013, **39**(4), 3691.

13 I. Mindru, G. Marinescu, D. Gingasu, L. Patron, L. Diamandescu, C. Ghica and B. Mironov, *Material Science and Engineering: B*, 2010, **170**(1-3), 99.

14 B.S. Barros, P.S. Melo, R.H.G.A. Kiminami, A.C.F.M. Costa, G.F. de Sa and S. Alves Jr., *Journal of Materials Science*, 2006, **41**(15), 4744.

15 Z. Lou and J. Hao, *Thin Solid Films*, 2004, **450**(2), 334.

16 K.H. Winbow and J. Cowley, *Ceramic Engineering and Science Proceedings*, 1996, **17**(1), 102.

17 R.F. Cooley and J.S. Reed, *Journal of the American Ceramic Society*, 1972, **55**, 395.

18 J. Popovic, E. Tkalcec, B. Grzeta, S..Kurajica and B. Rakvin, *American Mineralogist*, 2009, **94**, 771.

19 J.C. Waerenborgh, M.O. Figueiredo, J.M.P. Cabral and L.C.J. Pereira, *Journal of Solid State Chemistry*, 1994, **111**(2), 300.

20 A. LeNestour. *Corrélation structure-propriétés d'absorption UV-Vis-IR associée aux états de valence du cuivre dans des oxydes à base de zinc de type spinelle et würtzite*. PhD thesis, Université Bordeaux 1, avril 2006.

21 H. Matsui, C.-N. Xu, Y. Liu and H. Tateyama. *Physical Review B*, 2004, **69**, 235109.

22 N.J. van der Laag, M.D. Snel, P.C.M.M. Magusin and G. de With, *Journal of the European Ceramic Society*, 2004, **24**(8), 2417.

23 M. Vasile, P. Vlazan, and N.M. Avram, *Journal of Alloys and Compounds*, 2010, **500**(2), 185.

24 L. Torkian, M.M. Amini and Z. Bahrami, *Journal of Inorganic Materials*, 2011, **26**(5), 550.

25 V. Singh, R.P.S. Chakradhar, J.L. Rao and Dong-Kuk Kim, *Journal of Luminescence*, 2008, **128**, 394.

26 M.P. Pechini, U.S. Patent No. 3231328, Jan., 1966.

27 L. Cornu, M. Gaudon, and V. Jubera, *Journal of Material Chemistry C*, 2013, **1**, 5419.

28 T. Koskentalo, M. Leskelä and L. Niinistö. *Materials Research Bulletin*, 1985, **20**(3), 265.

29 A. van Die, A.C.H.I. Leenaers, W.F. van der Weg and G. Blasse, *Materials Research Bulletin*, 1987, **22**, 781.

30 R. Mlcak and A.H. Kitai, *Journal of Luminescence*, 1990, **46**(6), 391.

31 G. Li, D. Geng, M. Shang, C. Peng, Z. Cheng and J. Lin, Journal of Materials Chemistry, 2011, **21**, 13334.

32 S. Geschwind, P. Kisliuk, M.P. Klein, J.P. Remeika and D.L.Wood. *Physical Review*, 1962, **126**, 1684.

33 S. Shionoya, W.M. Yen and H. Yamamoto, *Phosphor Handbook, Second Edition*. 2007.

34 U-C. Chung, J.L. Mesa, J.L. Pizarro, V. Jubera, L. Lezama, M.I. Arriortua and T. Rojo, *Journal of Solid State Chemistry*, 2005, **178**, 2913.

35 O. Matumura, *Journal of the Physical Society of Japan*, 1959, **14**(1), 108.

36 R. Stahl-Brada and W. Low, *Physical Review*, 1959, **116**(3), 561.

37 E. Friedman and W. Low, *Physical Review*, 1960, **120**(2), 408.

38 J.S. Shaffer, H.A. Farach and C.P. Poole Jr., *Physical Review B*, 1976, **13**(5), 1869.

39 C.P. Poole Jr., H.A. Farach and W.K. Jackson, *The Journal of Chemical Physics*, 1974, **61**(6), 2220.

40 B.T. Allen, *The Journal of Chemical Physics*, 1965, **43**(11), 3820.

41 P.B. Dorain, *Physical Review*, 1958, **112**(4), 1058.

42 V. Singh, R.P.S. Chakradhar, J. L. Rao, and K. Dong-Kuk, *Journal of Solid State Chemistry*, 2007, **180**, 2067.

43 S. Geschwind, P. Kisliuk, M.P. Klein, J.P. Remeika and D.L. Wood, *Physical Review*, 1962, **126**(5), 1684.

44 S. Tanaka, K. Mizushima and S. Ida, *Journal of the Physical Society of Japan*, 1978, **45**(1), 133.

45 A. Abragam and B. Bleaney, *Electron Paramagnetic Resonance of Transition ions*. Clarendon Press, 1970.

46 J. Su Kim, J. Su Kim, T. Wan Kim, S. Myung Kim and H. Lee Park, *Applied Physics Letters*, 2005, **86**, 091912.

Luminescence switch of Mn-Doped ZnAl$_2$O$_4$ powder with temperature

L. Cornu[a,b], M. Duttine[a,b,c,d], M. Gaudon*[a,b] and V. Jubera*[a,b]

Mn-doped ZnAl$_2$O$_4$ can show a red to green luminescence switch with thermal treatment and so potentialities as thermal sensing pigments.